Predictive evaluation of hydrogen diffusion coefficient on Pd(111) surface by path integral simulations using neural network potential

Yuta Kataoka [1,2,*] Jun Haruyama [3] Osamu Sugino [1,3] and Motoyuki Shiga [4,†]

[1]*Department of Physics, Graduate School of Science, The University of Tokyo, Hongo, Bunkyo-ku, Tokyo 113-0033, Japan*

[2]*Department of Precision Engineering, Graduate School of Engineering, Osaka University, Yamadaoka, Suita, Osaka 565-0871, Japan*

[3]*Institute for Solid State Physics, The University of Tokyo, Kashiwanoha, Kashiwa-shi, Chiba 277-8581, Japan*

[4]*Center for Computational Science and e-Systems, Japan Atomic Energy Agency, Chiba 277-0871, Japan*

(Received 5 May 2024; accepted 6 November 2024; published 2 December 2024)

Quantum diffusion of hydrogen (H) on palladium (Pd) (111) was studied using two types of path integral simulations: quantum transition state theory (QTST) and ring polymer molecular dynamics (RPMD). The use of an artificial neural network potential trained by density functional theory calculations has made it feasible to perform path integral simulations considering nuclear quantum effects (NQEs) of a many-body Pd-H system with *ab initio* accuracy. The QTST result has shown a clear non-Arrhenius behavior in the diffusion coefficient (D) of H below the temperature of 150–200 K due to the NQEs. Comparing the D on Pd surface and bulk Pd, it was found that surface and bulk diffusion are competitive at high temperature. Consistent with this, it was observed in the RPMD simulation at 800 K that a part of the quantum trajectories of H on the surface bifurcates to the Pd subsurface. As the temperature decreases, the surface diffusion becomes much faster than the bulk diffusion. Furthermore, distinct quantum behaviors of H were identified at the surface and within the bulk. The D values obtained from this study using a "flexible" Pd surface model differed considerably from those previously reported using "frozen" Pd surface models, indicating an important contribution from Pd vibrations coupled with H diffusion.

DOI: 10.1103/PhysRevResearch.6.043224

I. INTRODUCTION

It is believed that hydrogen (H) adsorbed on metal surfaces moves rapidly and exhibits high chemical activity. This concerns not only for surface physics such as fuel cells [1] and catalysis [2], but also for molecular synthesis in outer space [3]. Therefore, understanding the diffusion behavior of H on metal surfaces is of fundamental importance in a wide range of scientific fields [4].

Experimental measurements of H diffusion coefficients (D) have been reported for various metal surfaces including W(110) [5,6], W(111) [7], W(211) [8], Ni(100) [9–11], Ni(111) [11–13], Cu(001) [14], Pt(111) [15,16], and Rh(111) [17]. Non-Arrhenius behavior in the temperature dependence was observed clearly for some cases [5–8,11,12,14,16]. Considering the mechanism of H diffusion in bulk metals [18–20], this phenomenon can be explained as a crossover between thermal and tunneling diffusion. This crossover is attributed to the lightweight nature of H atoms, which are expected to exhibit prominence at high temperatures for thermal diffusion and at low temperatures for tunneling diffusion, respectively. However, the data available for D on the metal surfaces are limited compared to those in bulk metals. For this reason, there has long been a need for theoretical predictions that allow a quantitative estimation of D consistently for both metal surfaces and bulk metals.

Computational analysis of H diffusion that considers both thermal and tunneling diffusion processes requires finite-temperature quantum simulations that account for nuclear quantum effects (NQEs) [21]. So far, many studies of H diffusion have relied on empirical potential models [22–33], such as the embedded atom method (EAM) [34,35]. Meanwhile, because of the computational effort required, the use of *ab initio* potential energy surface has mostly been limited to reduced dimensional theories [29,36–42].

It is now possible to simulate H on metal surfaces on the fly with the considered NQEs [43–45]; however, they are still computationally very expensive. Recently, full-dimensional modeling has become available owing to the introduction of machine-learning artificial neural network potential (NNP) that can mimic the potential energy surface (PES) of density functional theory (DFT) calculations [46–48]. This technique has paved the way for conducting quantum molecular dynamics simulations of many-body systems based on *ab initio* theory. Quantum dynamics on metal surfaces now appears to be one of the state-of-the-art applications of machine-learning potentials including NNPs [49–57].

In this paper, we study H diffusion on the (111) surface of face-centered-cubic (fcc) palladium (Pd), a commonly used

*Contact author: y.kataoka@prec.eng.osaka-u.ac.jp

†Contact author: shiga.motoyuki@jaea.go.jp

H storage metal. It is known that when molecular H approaches the Pd surface, it is exothermically chemisorbed as a single H atom. The adsorption energy on the Pd(111) surface is estimated to be about 1 eV per H_2 molecule in both experiments and DFT calculations [58–61]. According to DFT calculations, it is predicted that the Pd(111) surface has the most stable fcc site and the next most stable hcp (hexagonal close packed) site [42,62–65], and that H atoms move rapidly on the surface by jumping among these stable sites. However, there have been no reports on actual measurements of D so far. Furthermore, computational studies on the quantitative evaluation of D on the Pd(111) surface remain somewhat controversial, in particular, with respect to the thermal-to-tunneling crossover temperature [24,38,42,66]. Recently, velocity-resolved kinetics measurement was conducted for process in which H atoms collide on the Pd surface to form H molecules [61]. The rate of this recombinative desorption was reported to be competitive with the H diffusion into the subsurface and bulk Pd at high-temperature conditions. This implies that surface diffusion and bulk diffusion compete with each other at high temperatures in this system.

For the predictive evaluation of D, we have herein carried out quantum path integral (PI) simulations in multidimensional space using the NNPs. Specifically, we have used quantum transition state theory (QTST) [67,68] based on the combination of path integral molecular dynamics (PIMD) [69,70] and thermodynamic integration, incorporating quantum tunneling and zero-point effect that may become effective in the low-temperature regime. We have also used semiclassical ring polymer molecular dynamics (RPMD) [71–73] which incorporates anharmonic phonon vibrations that may become effective in the high-temperature regime, in addition to the quantum tunneling and zero-point effects. Recent PI simulations with NNPs have been successful in quantitatively evaluating the D of bulk Pd for a wide temperature range [49]. In fact, it was very recently reported that experimental measurement of the D of bulk Pd excellently agreed the simulation results [74]. We emphasize that our multidimensional QTST handles coordinates of all the atoms comprising the Pd-H system [75]. This differs from the three-dimensional (3D) QTST, depending only on the H coordinates, which was employed in earlier works of this system [24,38,42].

This technological advance not only provides a systematic analysis on the H diffusion mechanism, but also allows for a quantitative comparison of the D between the surface and bulk phases. Our computational results at low temperature indicate that the D of Pd surface is larger than that of bulk Pd, due to the different magnitude of NQEs affecting the H on Pd surface and in bulk Pd. At high temperature, the D of Pd surface and bulk Pd become the same order of magnitude, which means that the surface and bulk diffusion can compete with each other. In accordance to this finding, it was observed that the surface diffusion pathways in the RPMD simulations were partially split into the subsurface at high temperatures. The possibility of subsurface diffusion has been discussed theoretically before, and this paper demonstrates the quantum path integral trajectory of H diffusion on a metal subsurface.

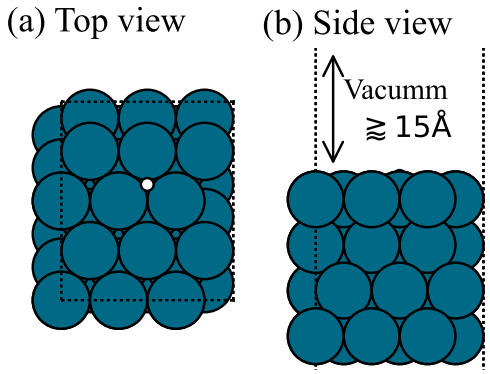

FIG. 1. Computational model used in this study. White and indigo spheres represent H and Pd atoms, respectively. (a) Shows the model viewed perpendicular to the surface, and (b) shows the model viewed from the side.

II. METHODS

A. System and DFT setups

As depicted in Fig. 1, we used a model system of H on the Pd(111) surface contained in a supercell with a lateral size of $3 \times 2\sqrt{3}$ in the units of the Pd interatomic distance. The system consists of a single H atom and 48 Pd atoms comprising a slab with 4 layers of 12 Pd atoms, each of which are separated by a vacuum of more than 15 Å. This model was used for all calculations in this paper. From DFT calculations of the bulk Pd using Perdew-Burke-Ernzerhof (PBE) exchange-correlation functional [76] with the k-point sampling of $24 \times 24 \times 24$, the Pd lattice constant for the supercell was determined to be $a_{\rm fcc} = 3.94$ Å. (For the sake of computation, this is somewhat shifted from the experimental value of $a_{\rm fcc} = 3.859$ Å [77].)

DFT calculations based on PBE functional were performed using the Vienna *ab initio* simulation package (VASP) software [78–80]. Projector augmented wave method [81] was used with a plane-wave cutoff at 300 eV, k-point sampling of $4 \times 4 \times 1$, and Gaussian smearing of the Fermi surface with a width of $\sigma = 0.04$ eV. In preparing the NNP reference data, it was useful to estimate the energy values without the effect of Gaussian smearing. For this purpose, the effect of electronic entropy was removed by the extrapolation $\sigma \to 0$.

B. Neural network potential

We constructed and applied a Behler-Parrinello–type NNP [46] using the Atomic Energy Network (AENET) software [82–84]. Here, we employed the Chebyshev descriptors for atomic environments implemented in AENET [82]. Chebyshev polynomial expansions were set to an order of 16 for the radial distribution functions and 4 for the angular distribution functions, with the cutoff radii for both functions being 5.5 Å. We used 2 hidden layers, 15 nodes in each hidden layer, and tanh with linear twisting for activation functions [82].

The NNP was trained using a data set comprising DFT calculated energy values for various configurations of the system outlined in Sec. II A. It is known that the energy of the structures of nontrained or with small number of data sets, such as transition state, are difficult to reproduce [85,86]. To

overcome this problem, we used self-learning hybrid Monte Carlo (SLHMC) method [87] to efficiently sample the data set from the target canonical ensemble in an automated manner. Based on dual-level hybrid Monte Carlo approach [88–90], the acceptance of a proposed trial move from a Newtonian trajectory on the NNP energy is determined by the Metropolis algorithm according to its probability on the DFT energy. While the structure was sampled, the NNP was trained and improved on the fly, making the move acceptable with longer trajectory [91].

Three different structures were prepared in which H atom is placed at fcc, hcp, and atop sites on the Pd(111) with the flexible surface model. The SLHMC simulations were then started independently from these structures. The temperature was gradually increased from 80 to 100, 300, 500, 800, and 1000 K to sample a balance of low- and high-energy structures. During the SLHMC simulations at high temperatures, H atoms were spontaneously sampled from the Pd subsurface as well as the Pd surface. A data set of 25 017 structures was selected in the final step of NNP training. On the data sets, 10% of were used for testing and the rest for training. The final training phase underwent an optimization process spanning 34 850 epochs, utilizing the limited-memory Broyden-Fletcher-Goldfarb-Shanno (L-BFGS) algorithm [92].

C. Ring polymer molecular dynamics

The imaginary-time PI simulation [69,93,94] is based on the isomorphism that the canonical ensemble of a quantum particle can be represented by that of P identical classical particles, the so-called "beads," that comprise a ring polymer with harmonic interactions next to each other in imaginary time. For a system with N quantum particles, the partition function can be expressed as

$$Z = \mathrm{tr}[e^{-\beta(\hat{T}+\hat{V})}], \tag{1}$$

where $\beta = 1/k_{\mathrm{B}}T$ with the Boltzmann constant $k_{\mathrm{B}}T$ and temperature T, $\hat{T}$ and $\hat{V}$ are the kinetic and potential energy operators. This can be formally rewritten, in the large-P limit, as an integral over the coordinate $\boldsymbol{x}$ with components $x_s^{(j)}$, with $s = 1 \ldots 3N$ (for a three-dimensional system) and $j = 1 \ldots P$, as

$$Z \propto \int \mathrm{d}\boldsymbol{x}\, e^{-\beta_P U_P(\boldsymbol{x})}, \tag{2}$$

where $\beta_P = \beta/P$, and

$$U_P(\boldsymbol{x}) = \sum_{j=1}^{P}\left[\sum_{s=1}^{3N}\frac{m_s}{2(\beta_P\hbar)^2}\left(x_s^{j+1}-x_s^{j}\right)^2 + V(\boldsymbol{x}_j)\right] \tag{3}$$

is an effective potential, and $m_{3n-2} = m_{3n-1} = m_{3n}$ is the mass of nth particle.

Canonical ensemble for this classical system can be generated from molecular dynamics (MD) associated with the effective Hamiltonian

$$H_P(\boldsymbol{x},\boldsymbol{p}) = \sum_{j=1}^{P}\sum_{s=1}^{3N}\frac{p_s^{(j)2}}{2m_s} + U_P(\boldsymbol{x}), \tag{4}$$

where $p_s^{(j)}$ represent the momentum conjugate to $x_s^{(j)}$. The RPMD method proposed by Craig and Manolopoulos corresponds to the Hamiltonian dynamics using Eq. (4) [71]. The time correlation function from the RPMD trajectory can be regarded as an approximation of the quantum (Kubo-transformed) canonical correlation function. In fact, the RPMD method is exact for position and velocity autocorrelations of harmonic oscillators. The RPMD is correct in the limits of high-temperature, classical, and short time [95].

The H diffusion coefficient can be computed from RPMD trajectories using the Einstein relation [21]

$$D = \frac{1}{2d}\lim_{t\to\infty}\frac{\left\langle\left[\boldsymbol{x}_{\mathrm{H}}^{c}(t)-\boldsymbol{x}_{\mathrm{H}}^{c}(0)\right]^2\right\rangle}{t}, \tag{5}$$

where the dimensional parameter is $d = 2$ for surface diffusion. The centroid coordinate of the H atom is defined as

$$\boldsymbol{x}_{\mathrm{H}}^{c}(t) = \frac{1}{P}\sum_{j=1}^{P}\boldsymbol{x}_{\mathrm{H}}^{(j)}(t), \tag{6}$$

where $\boldsymbol{x}_{\mathrm{H}}^{(j)}$ is the Cartesian coordinate of the jth bead of the H atom.

For H diffusion in bulk metals, the RPMD method was successfully applied to Pd by Kimizuka *et al.* [49], and to Nb, Fe, and W by Kwon *et al.* [52].

D. Quantum transition state theory

In the QTST proposed by Gillan [67,68], the free-energy profile is calculated as a reversible work necessary to move the centroid coordinates from site to site. An extension of the QTST was proposed by Shiga and Fujisaki [75] to generalize Fukui's intrinsic reaction coordinate defined in the mass-weighted coordinate space [96]. Thereby the free-energy surface is defined as

$$F(\boldsymbol{q}) = -\frac{1}{\beta}\log\rho(\boldsymbol{q}), \tag{7}$$

where

$$\rho(\boldsymbol{q}) = \prod_{s=1}^{3N}\left\langle\delta\left(q_s-\sqrt{m_s}x_s^{c}\right)\right\rangle \tag{8}$$

is the centroid probability with respect to the mass-weighted coordinates $\sqrt{m_s}x_s^{c}$. The free energy at the transition state (TS) is estimated by the thermodynamic integration from a minimum site (A) as

$$F_{\mathrm{TS}} = F_{\mathrm{A}} + \int_{\mathrm{A}}^{\mathrm{TS}} d\boldsymbol{q}\,\nabla F(\boldsymbol{q}), \tag{9}$$

where the free-energy gradient $\nabla F(\boldsymbol{q})$ corresponds to the negative value of the mean force applied to the centroid when it is constrained to a reaction coordinate $\boldsymbol{q}$. Accordingly, the gradient $\nabla F(\boldsymbol{q})$ is computed by constrained PIMD simulations at $\boldsymbol{q}$. In our QTST, the jump rate from site A to site B via TS is given by

$$\Gamma_{\mathrm{A}\to\mathrm{B}} = \frac{1}{\sqrt{2\pi\beta}}\frac{e^{-\beta(F_{\mathrm{TS}}-F_{\mathrm{A}})}}{\int_{\mathrm{A}} d\boldsymbol{q}\, e^{-\beta(F(\boldsymbol{q})-F_{\mathrm{A}})}}, \tag{10}$$

where the mass dependence is included in $\boldsymbol{q}$, as opposed to the original expression by Voth, Chandler, and Miller [97] and by Mills, Jónsson, and Schenter [98]. Thus, Eq. (10) enables a natural application of QTST to multidimensional reaction coordinates when phonon-coupled H diffusion is taken into account [75]. Assuming that the jumps are uncorrelated and adhere to a Markov process, with a transmission coefficient of unity, the diffusion coefficient is estimated as [99]

$$D = \frac{\ell_0^2}{d} \frac{\Gamma_{\mathrm{A}\to\mathrm{B}}\Gamma_{\mathrm{B}\to\mathrm{A}}}{\Gamma_{\mathrm{A}\to\mathrm{B}} + \Gamma_{\mathrm{B}\to\mathrm{A}}}, \tag{11}$$

where $\ell_0 = a_{\mathrm{fcc}}/\sqrt{2}$ is the distance between the surface atoms. In the classical transition state theory (TST), Eq. (10) is approximated as

$$\Gamma_{\mathrm{A}\to\mathrm{B}} = \frac{1}{\sqrt{2\pi\beta}} \frac{\mathrm{e}^{-\beta(V_{\mathrm{TS}}-V_{\mathrm{A}})}}{\int_{\mathrm{A}} d\boldsymbol{q}\, \mathrm{e}^{-\beta[V(\boldsymbol{q})-V_{\mathrm{A}}]}}. \tag{12}$$

For H diffusion in bulk metals, the QTST method was successfully applied to Pd, Al, Ag, and Cu by Kimizuka *et al.* [49,100,101], and to Nb, Fe, and W by Kwon *et al.* [52].

E. Thermal diffusion rate

For comparison, we calculated one-dimensional (1D) thermal diffusion rate (TDR) [40] along the minimum energy path connecting the fcc and hcp sites. D is obtained from Eq. (11) using the relationship

$$\Gamma_{\mathrm{A}\to\mathrm{B}} = \sqrt{\frac{\beta}{2\pi m \ell_{\mathrm{A}}^2}} \int_0^\infty P_{\mathrm{A}\to\mathrm{B}}(E) e^{-\beta E} dE, \tag{13}$$

where ℓ_{A} is the basin width of site A, and $P_{\mathrm{A}\to\mathrm{B}}(E)$ is the transmission probability from the initial basin minimum (A) to the final basin minimum (B). For a given kinetic energy E, semiclassical transmission probability is estimated by the Gamov method

$$P_{\mathrm{A}\to\mathrm{B}}(E) = \begin{cases} 0 \;\; (E \leqslant \max[0, V_{\mathrm{B}} - V_{\mathrm{A}}]) \\ e^{-\frac{2}{\hbar}\int_a^b dx \sqrt{2m[V(x)-V_{\mathrm{A}}-E]}} \\ \quad (\max[0, V_{\mathrm{B}} - V_{\mathrm{A}}] < E < V_{\mathrm{TS}} - V_{\mathrm{A}}) \\ 1 \;\; (E \geqslant V_{\mathrm{TS}} - V_{\mathrm{A}}), \end{cases} \tag{14}$$

where $x = a$ and b are the turning points in basins A and B, respectively, such that $V(a) = V(b) = E + V_{\mathrm{A}}$.

The detailed balance condition requires that the equilibrium population of the A and B sites are proportional to $\Gamma_{\mathrm{B}\to\mathrm{A}}$ and $\Gamma_{\mathrm{A}\to\mathrm{B}}$, respectively. Equation (14) obeys the relationship $P_{\mathrm{A}\to\mathrm{B}}(E' - V_{\mathrm{A}}) = P_{\mathrm{B}\to\mathrm{A}}(E' - V_{\mathrm{B}})$, so that from Eq. (13) we obtain $\Gamma_{\mathrm{A}\to\mathrm{B}}\ell_{\mathrm{A}} e^{-\beta V_{\mathrm{A}}} = \Gamma_{\mathrm{B}\to\mathrm{A}}\ell_{\mathrm{B}} e^{-\beta V_{\mathrm{B}}}$. This indicates that the populations of A and B are naturally Boltzmann distributions, proportional to $\ell_{\mathrm{A}} e^{-\beta V_{\mathrm{A}}}$ and $\ell_{\mathrm{B}} e^{-\beta V_{\mathrm{B}}}$, respectively.

F. Simulation setup

PIMD, RPMD, and QTST simulations using NNPs were performed by the PIMD software [102,103], for the same system as described in Sec. II A. We basically use a "flexible surface model" in which the top two Pd layers are allowed to move and the bottom two Pd layers frozen at the crystal lattice arrangement. This differs from a "relaxed surface model" in that the Pd positions are not fully optimized. For comparison we also tested a "frozen surface model" in which all Pd atoms are frozen at the crystal lattice arrangement. Generalized least-squares method was used to analyze the error in the mean-square displacement of the RPMD trajectories [104].

A series of PIMD and RPMD simulations were performed at temperatures of 200, 300, 400, 600, and 800 K with a step size of 0.25 fs using $P = 32$ beads. We also performed simulations at temperatures of 150, 100, and 80 K, however, D could not be converged due to the small number of diffusion. Starting from the structure sampled in the SLHMC calculations, PIMD simulations were performed for a length of 10 ps with the temperature controlled using the massive Nosé-Hoover chain method [105]. The final positions and velocities of the PIMD simulations were then used as initial input for the RPMD simulation of 250 ps long. The pair of PIMD and RPMD simulations was repeated 24 times in each case to gain statistics.

The QTST simulations were performed by running independent PIMD runs with centroid constraints at 12 different positions $\boldsymbol{q}$ along the minimum energy path (MEP) connecting the fcc and hcp sites on the Pd (111) surface. They were performed at temperatures 60, 70, 80, 100, and 150 K with 64 beads, and 200, 300, 400, 500, 600, 700, and 800 K with 32 beads. Each trajectory with a centroid constraint was 25–100 ps long to calculate a converged value of free-energy gradient. The computational time spent in this study is summarized in Table S1 in the Supplemental Material [107].

TABLE I. Energy and harmonic frequencies in meV. The angular frequency ω_α is defined such that $\frac{1}{2}\hbar\omega_\alpha$ is the harmonic zero-point energy. Imaginary frequencies are indicated by i×.

Site	V	$\hbar\omega_1$, $\hbar\omega_2$, $\hbar\omega_3$
fcc	0.0	127.1, 106.6, 105.1
Bridge	147.2	151.7, 149.2, i × 42.7
hcp	43.5	120.8, 107.5, 104.8
Atop	558.8	250.8, i × 16.9, i × 18.8

III. RESULTS AND DISCUSSIONS

A. Density functional theory

The DFT energies and vibrational frequencies of the Pd(111) surface sites are summarized in Table I. In this context, the energy values are shown relative to the fcc site which is the most stable site. The hcp site is the second most stable site, while the atop site is unstable, corresponding to a second-order saddle point. The fcc and hcp sites are connected through a transition state corresponding to the first saddle point.

B. Neural network potential

Figure 2 shows a comparison of the DFT and NNP energies of the test and training data sets, after the final NNP training was done as described in Sec. II B. The mean absolute error and root-mean-square error were found to be 0.299 (0.319) meV/atom and 0.448 (0.479) meV/atom, respectively, for the training set (test set). The comparison of the force predicted

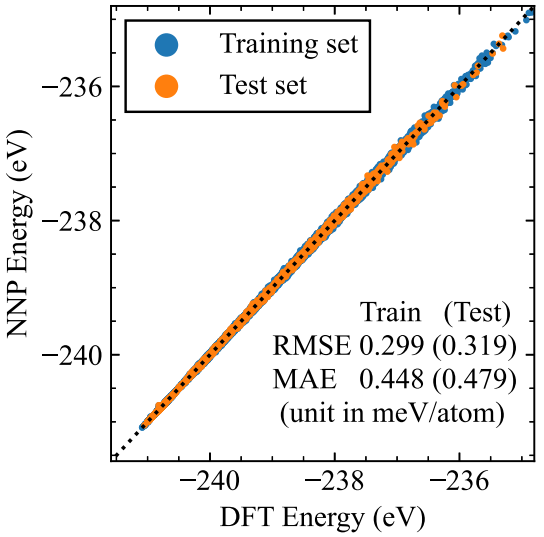

FIG. 2. Scatter plots of density functional theory (DFT) and neural network potential (NNP) energies of the total system that consists of $Pd_{48}H$. Blue and orange dots represent the energies of the training and test sets, respectively. The black dotted line indicates the function $y = x$.

from NNP and calculated from DFT is shown in Fig. S4 in the Supplemental Material [107]. The maximum absolute error of the energy ratio was found to be 6.01×10^{-4} (6.03×10^{-4}) for the training set (test set).

Figure 3 illustrates a comparison of the energy profiles obtained from DFT and NNP along the MEP from the fcc to hcp sites on the Pd(111) surface. The energy profile of NNP is in excellent agreement with that of DFT. In NNP, the hcp and bridge sites have energies that are 42.8 and 147.0 meV higher than the fcc site, respectively, which are in good agreement with the DFT results, 43.5 and 147.2 meV, respectively, as shown in Table I. Figure 4 compares the PES of H on Pd(111) surface calculated from DFT and NNP. The PES of DFT and NNP were found to be very similar to each other, both for the relaxed and frozen surface. In NNP, the atop site was

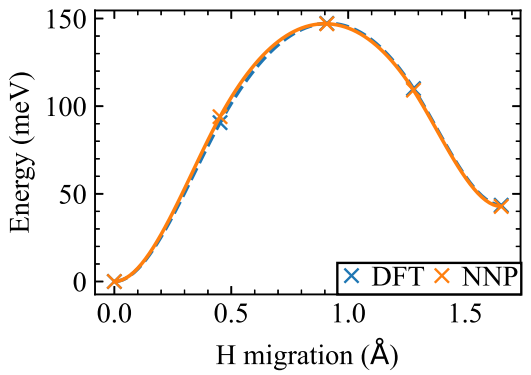

FIG. 3. Comparison of neural network potential (NNP, orange) and density functional theory (DFT, blue) energies along the minimum energy path. The results were obtained by the climbing-image nudged elastic band method [106] with the relaxed Pd model. The positions $x = 0.0$, 0.9, and 1.6 Å correspond to the fcc, bridge, and hcp sites, respectively.

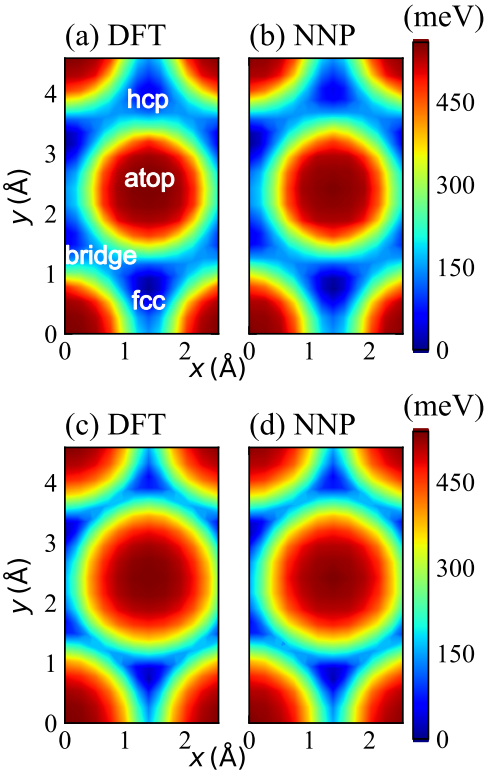

FIG. 4. The potential energy surface (PES) contours of H on Pd(111) surface obtained from (a) density functional theory and (b) neural network potential energies for the frozen surface model. (c), (d) Show the same PES contours as (a) and (b), respectively, but for the relaxed surface model. For the fixed surface, at each (x, y) mesh point, only the H position is optimized in the perpendicular direction of the surface, while for the relaxed surface model, positions of Pd in the top two layers are optimized. The error map is shown in Fig. S1 in the Supplemental Material [107].

557.6 meV higher in energy than the fcc site, in good agreement with the DFT result, 558.8 meV, as shown in Table I. The force acting on H atom along the minimum energy path is compared in Fig. S5 in the Supplemental Material [107].

More accuracy tests on the NNP are shown in the Supplemental Material [107]. Figure S2 shows those with respect to the displacement of surface Pd atom in Fig. S3, and Table S2 shows those with respect to the H vibrational zero-point energies (ZPEs). The ZPE errors in the comparison with DFT were smaller than 5.3 meV.

The SLHMC trajectories at 1000 K are displayed in Fig. S6 in the Supplemental Material. This shows that the structures of local minima (fcc and hcp sites) and transition state (bridge site) are covered, and they are then added to the NNP training data sets. As a reference, Fig. S7 in the Supplemental Material compares the acoustic phonon dispersion curves of fcc Pd between those computed using DFT and NNP optimized for bulk Pd system [49].

C. Diffusion coefficient

The calculated values of D from the QTST, RPMD, and MD simulations are summarized in Table II. The results compared with the classical TST results are plotted in Fig. 5 .

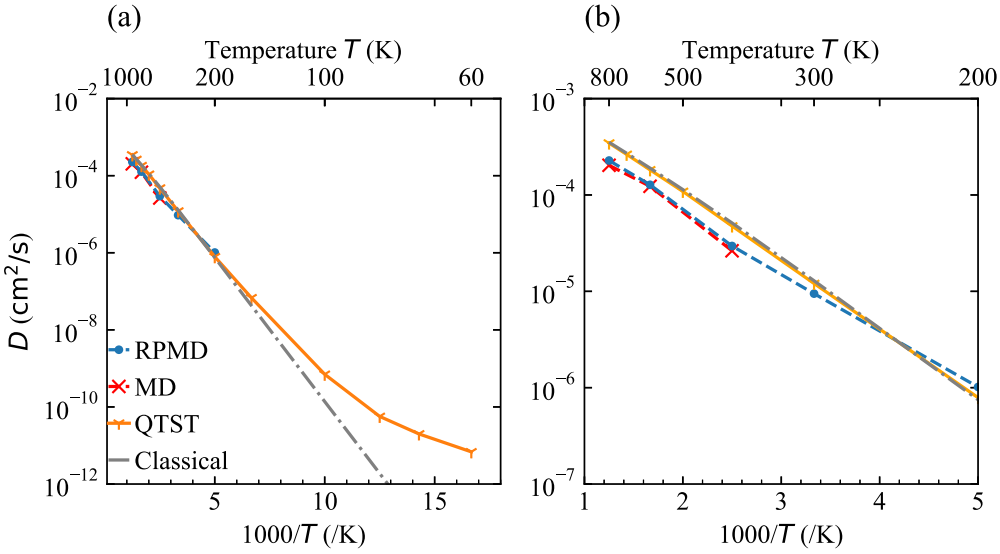

FIG. 5. Hydrogen diffusion coefficients (D) on Pd(111) surface obtained from classical transition state theory (gray), ring polymer molecular dynamics (blue), classical molecular dynamics (red), and quantum transition state theory (orange). (b) Shows the temperature of 800–200K of (a).

The classical TST shows almost perfect Arrhenius behavior (straight line) with the slope of $-\frac{\partial}{\partial\beta}\log D = 146.9$ meV and the $T \to \infty$ intercept of $D_\infty = 3.4 \times 10^{-3}$ cm^2/s. These values are reasonable since they are in the same order of magnitude as their static estimates in the classical regime. Using the activation energy from the bridge site to the fcc site and the reactive frequency of the fcc site ($\omega_r = 105.1$ meV), we obtain roughly $-\frac{\partial}{\partial\beta}\log D \approx 147.2$ meV and $D_\infty \approx \frac{\ell_0^2}{2}\frac{\omega_r}{2\pi} = 9.9 \times 10^{-3}$ cm^2/s. In contrast, the calculated values of D of QTST and RPMD showed non-Arrhenius behavior. The QTST result agrees well with that of classical TST at high temperatures, but it deviates significantly at low temperatures where the crossover from thermal to tunneling occurs. The crossover temperature T_c in which D of QTST departs from that of classical TST is roughly 150–200 K. This is higher than a static estimation [40] $T_c^{\text{static}} = |\omega_{ts}|/2\pi k_B = 78.9$ K, where $|\omega_{ts}| = 42.7$ meV is the absolute value of the bridge-site imaginary frequency taken from Table I. This trend was previously observed in H diffusion of fcc bulk metals as well [50,52,100,101]. For temperatures higher than 300 K, the D of RPMD is smaller than that of QTST, due to the influence of barrier recrossing in RPMD. This trend was also seen in H diffusion in fcc and bcc bulk metals [52,101].

TABLE II. Hydrogen diffusion coefficients in cm^2/s.

T (K)	D (QTST)	D (RPMD)	D (MD)
60	6.9×10^{-12}		
70	2.0×10^{-11}		
80	5.7×10^{-11}		
100	7.0×10^{-10}		
150	6.8×10^{-8}		
200	7.9×10^{-7}	1.0×10^{-6}	
300	1.2×10^{-5}	9.5×10^{-6}	
400	4.7×10^{-5}	3.0×10^{-5}	2.6×10^{-5}
500	1.1×10^{-4}		
600	1.8×10^{-4}	1.3×10^{-4}	1.2×10^{-4}
700	2.6×10^{-4}		
800	3.5×10^{-4}	2.3×10^{-4}	2.0×10^{-4}

In Fig. 6, the D obtained from the multidimensional QTST with the flexible surface model is compared with those obtained from the 3D QTST and 1D TDR with the frozen surface model. The 3D QTST calculation, in which the effect of Pd vibrations is switched off, overestimates D by a factor of 1.5–6.0 compared to the multidimensional QTST calculation. The 1D TDR calculation, in which both the effects of nonreactive zero-point motion of H (i.e., vibrational modes perpendicular to the diffusion pathway) and the Pd phonon vibrations are switched off, overestimates D by up to an order of magnitude compared to the multidimensional QTST calculation, especially at high temperatures. This confirms that the coupling of H diffusion to nonreactive zero-point motion and Pd vibrations play indispensable roles in the quantitative evaluation of the D, as pointed out earlier also by Nikitin *et al.* [38].

In Fig. 7 , the D obtained from RPMD and QTST are compared for H diffusion on the Pd(111) surface and within bulk Pd. Note that both of these results were obtained from the NNP, which was constructed using the same DFT functional, specifically PBE functional. [49,100]. At low temperatures, the bulk D is much smaller than that of surface diffusion. However, as the temperature increases, bulk and surface diffusion become more competitive. The D values of the bulk and surface diffusion are almost comparable at temperature 800 K. This explains why a part of RPMD trajectories bifurcates to the subsurface, as shown in Sec. III D.

It is important to point out the difference in the impact of NQE on surface and bulk H diffusion. To this end, energy barriers along the minimum energy path were qualitatively evaluated from static DFT-PBE calculations and ZPE corrections using the harmonic approximation. For surface diffusion, the energy barrier from the fcc site to the bridge site was the largest, estimated at 147.2 meV without the ZPE

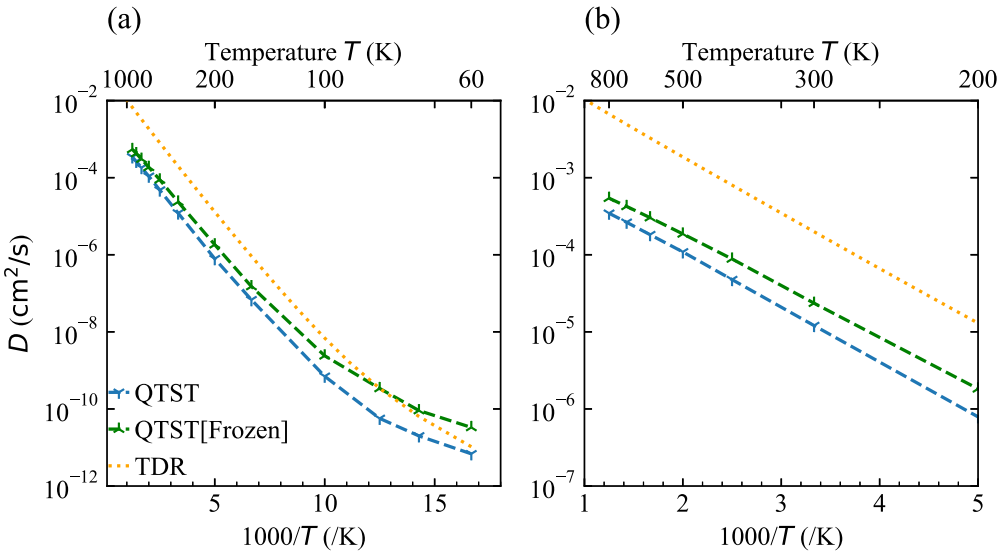

FIG. 6. Hydrogen diffusion coefficients (D) on Pd(111) surface obtained from quantum transition state theory (QTST) with flexible surface model (blue), QTST with frozen surface model (green), and one-dimensional thermal diffusion rate with frozen surface model (orange). (b) Shows the temperature of 800–200K of (a).

correction. In this case, the ZPE correction is negative at −16.1 meV. Thus, as the temperature decreases, the effective barrier is lowered by the zero-point energy and further lowered by tunneling. As a result, the temperature dependence of D has a C-shaped curve. (In fact, H diffusion in bulk Al is known to behave similarly to this type [101].) On the other hand, the largest energy barrier in bulk diffusion is the transition state on the way from octahedral to tetrahedral sites, which is estimated to be 160 meV without ZPE. In this case, the ZPE correction is positive at 112.3 meV, in contrast to the case of surface diffusion [108]. Thus, since the ZPE and tunneling effects compete with each other, the temperature dependence of D is no longer simple, and an inverse S-shaped curve is observed [49,100]. This is the reason why D differs significantly between surface and bulk diffusion at low temperatures.

D. Diffusion pathways

Figure 8 shows the centroid trajectories of H on the Pd(111) surface obtained from the RPMD simulations at 800 and 600 K. The trajectories obtained from classical MD are

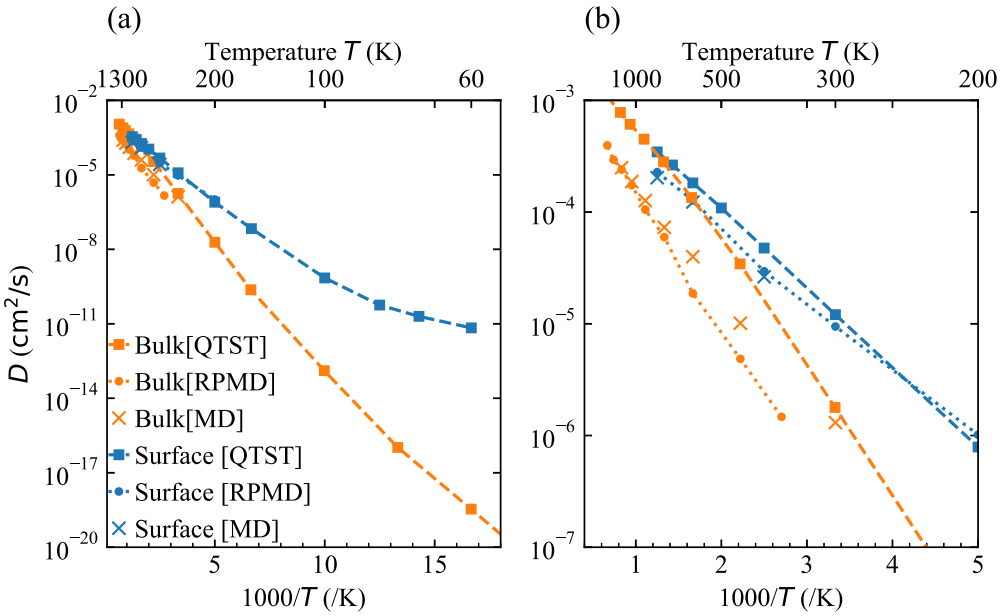

FIG. 7. Hydrogen diffusion coefficients (D) obtained from ring polymer molecular dynamics (circle), molecular dynamics (cross), and quantum transition state theory (square) on Pd(111) surface (blue) and in bulk Pd (orange) [49]. (b) Shows the temperature of 800–200K of (a).

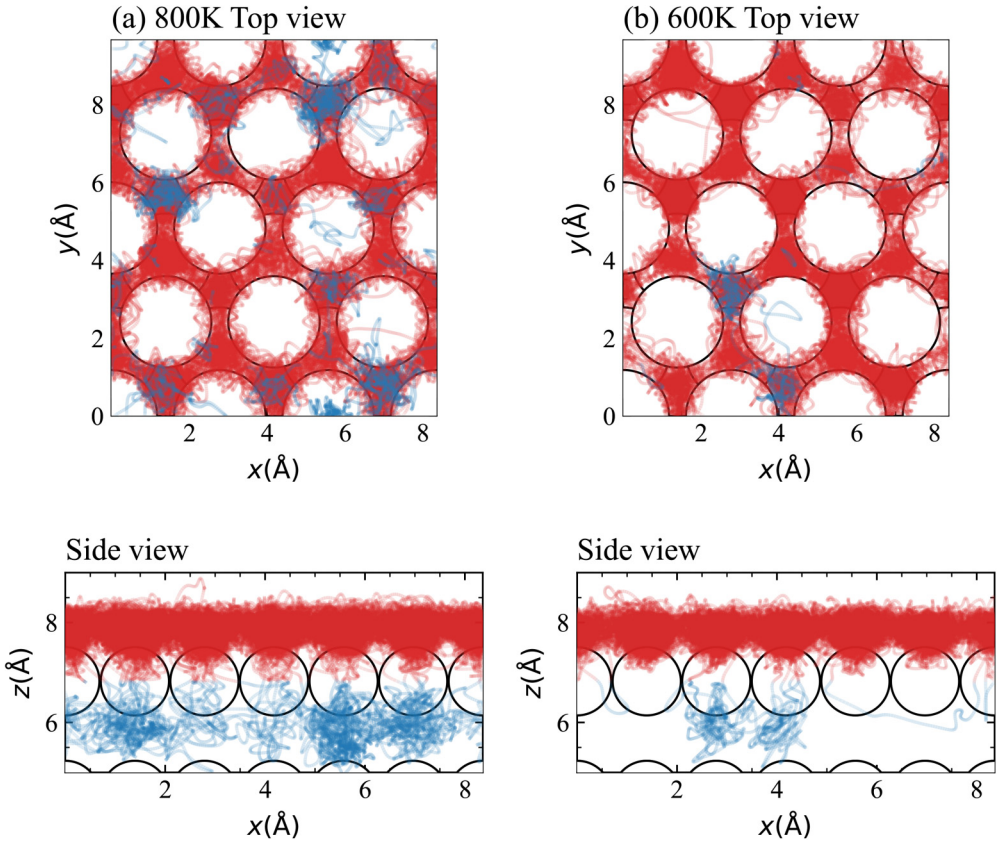

FIG. 8. Top and side views of trajectories of H atom obtained from RPMD simulations at (a) 800 K and (b) 600 K. The centroid coordinates of four 50-ps-long RPMD trajectories are superimposed. Red and blue lines are the trajectories that belong to the Pd(111) surface and subsurface, respectively. The white spheres are shown as a guide to the eye for their lattice positions of Pd atoms; the actual off-lattice positions of Pd atoms are not shown here.

shown in Fig. S8 in the Supplemental Material [107]. Here it can be seen that some of the surface trajectories are bifurcated into the subsurface. The trajectories colored red and blue correspond to the surface and subsurface trajectories, respectively. The subsurface trajectories appear more frequently at 800 than at 600 K, indicating that the competition between the surface and subsurface diffusion is greater at higher temperatures. In fact, this result seems to be consistent with the outcome from transient kinetic experiments by Schwarzer *et al.* [61] on thermal recombinative desorption rates of the HD molecule on Pd(111) and Pd(332) surfaces between 523 and 1023 K. Based on a kinetic model describing the competition between recombination of surface-adsorbed H and D (deuterium) atoms and their diffusion into the bulk, it was suggested that the HD formation rate cannot be reproduced by a kinetic model without considering a second-order reaction of bulk diffusion.

We found two types of trajectories that go through the subsurface. One dives from the fcc site into a subsurface site and returns to the same fcc site. The other dives from the fcc site into a subsurface site, then migrates to another subsurface site and returns to another surface site.

The octahedral (oh) site is where the subsurface trajectories visit most frequently, in agreement with the prediction from the static PES by Hong and Rahman [109], the H wavefunction calculations by Ozawa *et al.* [64], and kinetic Monte Carlo simulation by Ciufo and Henkelman [32]. According to the static DFT calculations employing the PBE functional, the energies of the subsurface oh site, and the transition state connecting the surface fcc and subsurface oh sites, are reported to be 340 and 350 meV, respectively [32].

E. Comparison with previous studies

In Fig. 9 , we compare our QTST and RPMD results with previous calculations of H diffusion on the Pd(111) surface reported by Rick, Lynch, and Doll [24] and Nikitin *et al.* [38]. Note that the comparison can only be made over limited temperature range for which previous data are available. Rick *et al.* studied the 100–300 K range based on the QTST and an EAM potential, where the NQE in the PI expression is approximated with an effective potential using Gaussian smearing. Nikitin *et al.* studied the 100–600 K range based on the quantum transition state wave packet method [110] (TSWP) and a DFT potential within the generalized gradient approximation. In these works, quantum simulations were performed on the 3D PES with respect to the H atom degrees of freedom, and thus the effect of Pd phonon vibrations was not considered. In addition, it was assumed in these calculations that fcc and hcp sites were energetically degenerate; note that Eq. (1) of the paper by Rick *et al.* becomes the same as Eq. (11) in this paper, if one assumes the reaction coordinate of H atom as $\boldsymbol{q} = \sqrt{m}\boldsymbol{x}_{\mathrm{H}}$, and uses the symmetry of jumping rates $\Gamma_{\mathrm{A}\to\mathrm{B}} = \Gamma_{\mathrm{B}\to\mathrm{A}}$ in Eq. (10).

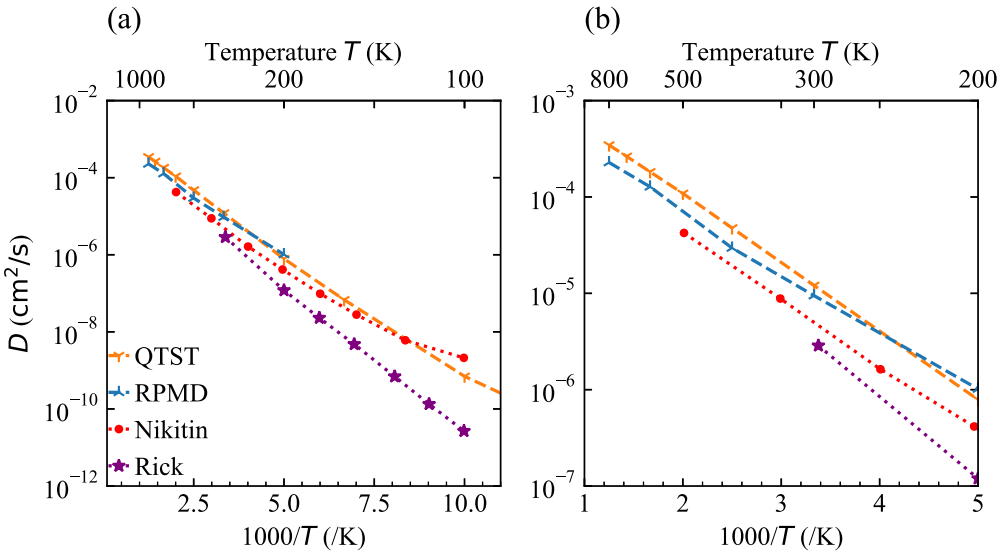

FIG. 9. Hydrogen diffusion coefficients (D) from RPMD (blue) and QTST (orange) from this study, and from previous studies by Nikitin *et al.* [38] (red) and Rick *et al.* [24] (violet). (b) Shows the temperature of 800–200K of (a).

The energy barrier for the H diffusion was estimated to be 202 meV by Rick *et al.* and 169 meV by Nikitin *et al.* These values are higher than those fitted from our RPMD and QTST simulations at high temperature, 125 and 147 meV, respectively. As a result, the D values reported by Rick *et al.* and Nikitin *et al.* are both smaller than our RPMD and QTST simulations.

As opposed to our study, Rick *et al.* did not find a clear non-Arrhenius behavior in D. On the other hand, Nikitin *et al.* did find the non-Arrhenius behavior, and their estimation of $T_c^{\mathrm{TSWP}} = 60-100$ K. This value is lower than our QTST estimate of $T_c = 150-200$ K.

IV. CONCLUSION

H diffusion on Pd(111) was investigated by multidimensional PI simulations using NNP with the DFT accuracy. Diffusion coefficients were determined by QTST across a broader temperature range than has been previously reported. The QTST data were then improved by RPMD simulations incorporating dynamic effects in the high-temperature regime. Non-Arrhenius behavior due to quantum tunneling effects was confirmed at low temperatures, consistent with some of the previous theoretical studies. However, the D calculated quantitatively exhibits deviations from those reported in previous studies. It is determined that at high temperatures, surface diffusion and bulk diffusion engage in competition, with diffusion pathways partially diverging into the subsurface. At low temperatures, however, surface diffusion was found to be much faster than bulk diffusion due to strong tunneling effects. The quantum effects associated with subsurface penetration will be the subject of further investigation in future studies. We hope that this study will stimulate new experiments on this system.

ACKNOWLEDGMENTS

This work was supported by JSPS KAKENHI Grant No. JP23KJ0429, and the New Energy and Industrial Technology Development Organization (NEDO) project. Part of the calculation was performed at the Supercomputer system B in the Institute for Solid State Physics, the University of Tokyo. M.S. thanks JSPS Grant-in-Aid for Scientific Research (Grants No. 23K04670, No. 23H01273, and No. 24K01145) for financial support. The PIMD software has been developed using the supercomputer facilities in JAEA. We thank Dr. B. Thomsen in JAEA and Prof. Y. Nagai in The University of Tokyo for discussion on SLHMC. We thank Associate prof. I. Hamada for the comments on the paper. The authors thank Prof. H. Kimizuka for providing us with the NNP optimized for bulk Pd system.

[1] K. Sakaushi, Quantum proton tunneling in multi-electron/-proton transfer electrode processes, Faraday Discuss. **221**, 428 (2020).

[2] W. J. Liu, B. L. Wu, and C. S. Cha, Surface diffusion and the spillover of H-adatoms and oxygen-containing surface species on the surface of carbon black and Pt/C porous electrodes, J. Electroanal. Chem. **476**, 101 (1999).

[3] N. Watanabe and A. Kouchi, Ice surface reactions: A key to chemical evolution in space, Prog. Surf. Sci. **83**, 439 (2008).

[4] *Hydrogenomics: The Science of Fully Utilizing Hydrogen*, edited by S. Orimo, K. Fukutani, and K. Fujita (Kyoritsu Shuppan Co. Ltd., Tokyo, 2023).

[5] R. DiFoggio and R. Gomer, Diffusion of hydrogen and deuterium on the (110) plane of tungsten, Phys. Rev. B **25**, 3490 (1982).

[6] S. C. Wang and R. Gomer, Diffusion of hydrogen, deuterium, and tritium on the (110) plane of tungsten, J. Chem. Phys. **83**, 4193 (1985).

[7] C. Dharmadhikari and R. Gomer, Diffusion of hydrogen and deuterium on the (111) plane of tungsten, Surf. Sci. **143**, 223 (1984).

[8] E. Daniels, J. Lin, and R. Gomer, Diffusion anisotropy of hydrogen and deuterium on the tungsten (211) plane, Surf. Sci. **204**, 129 (1988).

[9] S. George, A. DeSantolo, and R. Hall, Surface diffusion of hydrogen on Ni(100) studied using laser-induced thermal desorption, Surf. Sci. **159**, L425 (1985).

[10] D. Mullins, B. Roop, S. Costello, and J. White, Isotope effects in surface diffusion: Hydrogen and deuterium on Ni(100), Surf. Sci. **186**, 67 (1987).

[11] T. S. Lin and R. Gomer, Diffusion of ^{1}H and ^{2}H on the Ni(111) and (100) planes, Surf. Sci. **255**, 41 (1991).

[12] A. Lee, X. D. Zhu, A. Wong, L. Deng, and U. Linke, Observation of diffusion of H and D on Ni(111) from over-barrier hopping to nonactivated tunneling, Phys. Rev. B **48**, 11256 (1993).

[13] G. X. Cao, E. Nabighian, and X. D. Zhu, Diffusion of hydrogen on Ni(111) over a wide range of temperature: Exploring quantum diffusion on metals, Phys. Rev. Lett. **79**, 3696 (1997).

[14] L. J. Lauhon and W. Ho, Direct observation of the quantum tunneling of single hydrogen atoms with a scanning tunneling microscope, Phys. Rev. Lett. **85**, 4566 (2000).

[15] E. Seebauer and L. Schmidt, Surface diffusion of hydrogen on Pt(111): Laser-induced thermal desorption studies, Chem. Phys. Lett. **123**, 129 (1986).

[16] C. Z. Zheng, C. K. Yeung, M. M. T. Loy, and X. Xiao, Quantum diffusion of H on Pt(111): Step effects, Phys. Rev. Lett. **97**, 166101 (2006).

[17] E. Seebauer, A. Kong, and L. Schmidt, Surface diffusion of hydrogen and CO on Rh (111): Laser-induced thermal desorption studies, J. Chem. Phys. **88**, 6597 (1988).

[18] H. Wipf, *Hydrogen in Metals III: Properties and Applications*, (Springer, Berlin, 1997), Vol. 73, pp. 51–91.

[19] J. Völkl, G. Alefeld, Diffusion of hydrogen in metals in *Hydrogen in Metals I. Topics in Applied Physics*, edited by J. Völkl, G. Alefeld (Springer, Berlin, Heidelberg, 1978), Vol. 28, pp. 321–348.

[20] Y. Fukai, *The Metal-hydrogen System: Basic Bulk Properties*, 2nd ed. (Springer, Berlin, 2005), Vol. 21.

[21] J. D. Doll and A. F. Voter, Recent developments in the theory of surface-diffusion, Annu. Rev. Phys. Chem. **38**, 413 (1987).

[22] R. Jaquet and W. H. Miller, Quantum mechanical rate constants via path integrals: diffusion of hydrogen atoms on a tungsten (100) surface, J. Phys. Chem. **89**, 2139 (1985).

[23] B. M. Rice, B. C. Garrett, M. L. Koszykowski, S. M. Foiles, and M. S. Daw, Kinetic isotope effects for hydrogen diffusion in bulk nickel and on nickel surfaces, J. Chem. Phys. **92**, 775 (1990).

[24] S. W. Rick, D. L. Lynch, and J. D. Doll, The quantum dynamics of hydrogen and deuterium on the Pd(111) surface: A path-integral transition-state theory study, J. Chem. Phys. **99**, 8183 (1993).

[25] T. R. Mattsson, U. Engberg, and G. Wahnstrom, H diffusion on Ni(100): A quantum Monte Carlo simulation, Phys. Rev. Lett. **71**, 2615 (1993).

[26] Y.-C. Sun and G. A. Voth, Path integral calculation of hydrogen diffusion rates on metal surfaces, J. Chem. Phys. **98**, 7451 (1993).

[27] S. E. Wonchoba, W.-P. Hu, and D. G. Truhlar, Surface diffusion of H on Ni(100): Interpretation of the transition temperature, Phys. Rev. B **51**, 9985 (1995).

[28] R. Baer, Y. Zeiri, and R. Kosloff, Influence of dimensionality on deep tunneling rates: A study based on the hydrogen-nickel system, Phys. Rev. B **54**, R5287 (1996).

[29] T. R. Mattsson, G. Wahnström, L. Bengtsson, and B. Hammer, Quantum-mechanical calculation of H on Ni(001) using a model potential based on first-principles calculations, Phys. Rev. B **56**, 2258 (1997).

[30] Y. V. Suleimanov, Surface diffusion of hydrogen on Ni(100) from ring polymer molecular dynamics, J. Phys. Chem. C **116**, 11141 (2012).

[31] T. Yoshikawa, T. Takayanagi, H. Kimizuka, and M. Shiga, Quantum–thermal crossover of hydrogen and tritium diffusion in α-iron, J. Phys. Chem. C **116**, 23113 (2012).

[32] R. A. Ciufo and G. Henkelman, Embedded atom method potential for hydrogen on palladium surfaces, J. Mol. Model. **26**, 336 (2020).

[33] R. Baer and R. Kosloff, Quantum dissipative dynamics of adsorbates near metal surfaces: A surrogate Hamiltonian theory applied to hydrogen on nickel, J. Chem. Phys. **106**, 8862 (1997).

[34] M. S. Daw and M. I. Baskes, Embedded-atom method: Derivation and application to impurities, surfaces, and other defects in metals, Phys. Rev. B **29**, 6443 (1984).

[35] M. S. Daw, S. M. Foiles, and M. I. Baskes, The embedded-atom method: A review of theory and applications, Mater. Sci. Rep. **9**, 251 (1993).

[36] D. H. Zhang, J. C. Light, and S. Y. Lee, Transition state wave packet study of hydrogen diffusion on Cu(100) surface, J. Chem. Phys. **111**, 5741 (1999).

[37] J. Kua, L. J. Lauhon, W. Ho, and W. A. Goddard, III, Direct comparisons of rates for low temperature diffusion of hydrogen and deuterium on Cu(001) from quantum mechanical calculations and scanning tunneling microscopy experiments, J. Chem. Phys. **115**, 5620 (2001).

[38] I. Nikitin, W. Dong, H. F. Busnengo, and A. Salin, Diffusion of a hydrogen atom on the Pd(111) surface: Quantum transition state wave packet approach, Surf. Sci. **547**, 149 (2003).

[39] A. Nojima and K. Yamashita, A theoretical study of hydrogen adsorption and diffusion on a W(110) surface, Surf. Sci. **601**, 3003 (2007).

[40] W. Fang, J. O. Richardson, J. Chen, X. Z. Li, and A. Michaelides, Simultaneous deep tunneling and classical hopping for hydrogen diffusion on metals, Phys. Rev. Lett. **119**, 126001 (2017).

[41] A. R. Hopkinson and M. I. J. Probert, Quantum diffusion of H/D on Ni(111)-A partially adiabatic centroid MD study, J. Chem. Phys. **148**, 102339 (2018).

[42] Y. Kataoka, J. Haruyama, and O. Sugino, Theoretical calculation and comparison of H diffusion on Cu(111), Ni(111), Pd(111), and Au(111), Phys. Rev. B **107**, 205414 (2023).

[43] E. M. McIntosh, K. T. Wikfeldt, J. Ellis, A. Michaelides, and W. Allison, Quantum effects in the diffusion of hydrogen on Ru(0001), J. Phys. Chem. Lett. **4**, 1565 (2013).

[44] L. Yan, Y. Yamamoto, M. Shiga, and O. Sugino, Nuclear quantum effect for hydrogen adsorption on Pt(111), Phys. Rev. B **101**, 165414 (2020).

[45] J. Lan, V. V. Rybkin, and M. Iannuzzi, Ionization of water as an effect of quantum delocalization at aqueous electrode interfaces, J. Phys. Chem. Lett. **11**, 3724 (2020).

[46] J. Behler and M. Parrinello, Generalized neural-network representation of high-dimensional potential-energy surfaces, Phys. Rev. Lett. **98**, 146401 (2007).

[47] J. Behler, Constructing high-dimensional neural network potentials: A tutorial review, Int. J. Quantum Chem. **115**, 1032 (2015).

[48] J. Behler, Four generations of high-dimensional neural network potentials, Chem. Rev. **121**, 10037 (2021).

[49] H. Kimizuka, B. Thomsen, and M. Shiga, Artificial neural network-based path integral simulations of hydrogen isotope diffusion in palladium, J. Phys. Energy **4**, 034004 (2022).

[50] H. E. Sauceda, L. E. Gálvez-González, S. Chmiela, L. O. Paz-Borbón, K.-R. Müller, and A. Tkatchenko, BIGDML - Towards accurate quantum machine learning force fields for materials, Nat. Commun. **13**, 3733 (2022).

[51] K. Gu, C. Li, B. Jiang, S. Lin, and H. Guo, Short-and long-time dynamics of hydrogen spillover from a single atom platinum active site to the Cu(111) host surface, J. Phys. Chem. C **126**, 17093 (2022).

[52] H. Kwon, M. Shiga, H. Kimizuka, and T. Oda, Accurate description of hydrogen diffusivity in bcc metals using machine-learning moment tensor potentials and path-integral methods, Acta Mater. **247**, 118739 (2023).

[53] C. Li, Y. Li, and B. Jiang, First-principles surface reaction rates by ring polymer molecular dynamics and neural network potential: Role of anharmonicity and lattice motion, Chem. Sci. **14**, 5087 (2023).

[54] L. Zhang, J. Zuo, Y. V. Suleimanov, and H. Guo, Ring polymer molecular dynamics approach to quantum dissociative chemisorption rates, J. Phys. Chem. Lett. **14**, 7118 (2023).

[55] N. Gerrits, B. Jackson, and A. Bogaerts, Accurate reaction probabilities for translational energies on both sides of the barrier of dissociative chemisorption on metal surfaces, J. Phys. Chem. Lett. **15**, 2566 (2024).

[56] W. G. Stark, J. Westermayr, O. A. Douglas-Gallardo, J. Gardner, S. Habershon, and R. J. Maurer, Machine learning interatomic potentials for reactive hydrogen dynamics at metal surfaces based on iterative refinement of reaction probabilities, J. Phys. Chem. C **127**, 24168 (2023).

[57] W. G. Stark, C. van der Oord, I. Batatia, Y. Zhang, B. Jiang, G. Csányi, and R. J. Maurer, Benchmarking of machine learning interatomic potentials for reactive hydrogen dynamics at metal surfaces, Mach. Learn.: Sci. Technol. **5**, 030501 (2024).

[58] H. Conrad, G. Ertl, and E. Latta, Adsorption of hydrogen on palladium single crystal surfaces, Surf. Sci. **41**, 435 (1974).

[59] G. W. Watson, R. P. Wells, D. J. Willock, and G. J. Hutchings, A comparison of the adsorption and diffusion of hydrogen on the {111} surfaces of Ni, Pd, and Pt from density functional theory calculations, J. Phys. Chem. B **105**, 4889 (2001).

[60] H. Sakagami, M. Tachikawa, and T. Ishimoto, Hydrogen/deuterium adsorption and absorption properties on and in palladium using a combined plane wave and localized basis set method, Int. J. Quantum Chem. **120**, e26275 (2020).

[61] M. Schwarzer, N. Hertl, F. Nitz, D. Borodin, J. Fingerhut, T. N. Kitsopoulos, and A. M. Wodtke, Adsorption and absorption energies of hydrogen with palladium, J. Phys. Chem. C **126**, 14500 (2022).

[62] W. Dong, G. Kresse, J. Furthmüller, and J. Hafner, Chemisorption of H on Pd(111): An *ab initio* approach with ultrasoft pseudopotentials, Phys. Rev. B **54**, 2157 (1996).

[63] O. M. Løvvik and R. A. Olsen, Adsorption energies and ordered structures of hydrogen on Pd(111) from density-functional periodic calculations, Phys. Rev. B **58**, 10890 (1998).

[64] N. Ozawa, N. B. Arboleda, T. A. Roman, H. Nakanishi, W. A. Diño, and H. Kasai, Quantum states of hydrogen atom motion on the Pd(111) surface and in the subsurface, J. Phys.: Condens. Matter **19**, 365214 (2007).

[65] L. Kristinsdóttir and E. Skúlason, A systematic DFT study of hydrogen diffusion on transition metal surfaces, Surf. Sci. **606**, 1400 (2012).

[66] T. Firmino, R. Marquardt, F. Gatti, and W. Dong, Diffusion rates for hydrogen on Pd(111) from molecular quantum dynamics calculations, J. Phys. Chem. Lett. **5**, 4270 (2014).

[67] M. J. Gillan, Quantum-classical crossover of the transition rate in the damped double well, J. Phys. C: Solid State Phys. **20**, 3621 (1987).

[68] M. J. Gillan, Quantum simulation of hydrogen in metals, Phys. Rev. Lett. **58**, 563 (1987).

[69] M. Parrinello and A. Rahman, Study of an *F* center in molten KCl, J. Chem. Phys. **80**, 860 (1984).

[70] M. E. Tuckerman, B. J. Berne, G. J. Martyna, and M. L. Klein, Efficient molecular dynamics and hybrid Monte Carlo algorithms for path integrals, J. Chem. Phys. **99**, 2796 (1993).

[71] I. R. Craig and D. E. Manolopoulos, Quantum statistics and classical mechanics: Real time correlation functions from ring polymer molecular dynamics, J. Chem. Phys. **121**, 3368 (2004).

[72] I. R. Craig and D. E. Manolopoulos, Chemical reaction rates from ring polymer molecular dynamics, J. Chem. Phys. **122**, 084106 (2005).

[73] I. R. Craig and D. E. Manolopoulos, A refined ring polymer molecular dynamics theory of chemical reaction rates, J. Chem. Phys. **123**, 034102 (2005).

[74] T. Ozawa, H. Nakanishi, K. Kato, R. Shimizu, T. Hitosugi, and K. Fukutani, Observation of resonant tunneling of proton from octahedral to tetrahedral sites in Pd, J. Phys. Chem. Solids **185**, 111741 (2024).

[75] M. Shiga and H. Fujisaki, A quantum generalization of intrinsic reaction coordinate using path integral centroid coordinates, J. Chem. Phys. **136**, 184103 (2012).

[76] J. P. Perdew, K. Burke, and M. Ernzerhof, Generalized gradient approximation made simple, Phys. Rev. Lett. **77**, 3865 (1996).

[77] W. P. Davey, Precision measurements of the lattice constants of twelve common metals, Phys. Rev. **25**, 753 (1925).

[78] G. Kresse and J. Hafner, *Ab initio* molecular dynamics for liquid metals, Phys. Rev. B **47**, 558 (1993).

[79] G. Kresse and J. Furthmuller, Efficiency of *ab-initio* total energy calculations for metals and semiconductors using a plane-wave basis set, Comput. Mater. Sci. **6**, 15 (1996).

[80] G. Kresse and J. Furthmuller, Efficient iterative schemes for *ab initio* total-energy calculations using a plane-wave basis set, Phys. Rev. B **54**, 11169 (1996).

[81] G. Kresse and D. Joubert, From ultrasoft pseudopotentials to the projector augmented-wave method, Phys. Rev. B **59**, 1758 (1999).

[82] N. Artrith and A. Urban, An implementation of artificial neural-network potentials for atomistic materials simulations: Performance for TiO_2, Comput. Mater. Sci. **114**, 135 (2016).

[83] N. Artrith, A. Urban, and G. Ceder, Efficient and accurate machine-learning interpolation of atomic energies in compositions with many species, Phys. Rev. B **96**, 014112 (2017).

[84] A. M. Cooper, J. Kästner, A. Urban, and N. Artrith, Efficient training of ANN potentials by including atomic forces via Taylor expansion and application to water and a transition-metal oxide, Npj Comput. Mater. **6**, 54 (2020).

[85] A. Fantasia, F. Rovaris, O. Abou El Kheir, A. Marzegalli, D. Lanzoni, L. Pessina, P. Xiao, C. Zhou, L. Li, G. Henkelman, E. Scalise, and F. Montalenti, Development of a machine learning interatomic potential for exploring pressure-dependent kinetics of phase transitions in germanium, J. Chem. Phys. **161**, 014110 (2024).

[86] J. A. Vita and D. Schwalbe-Koda, Data efficiency and extrapolation trends in neural network interatomic potentials, Mach. Learn.: Sci. Technol. **4**, 035031 (2023).

[87] Y. Nagai, M. Okumura, K. Kobayashi, and M. Shiga, Self-learning hybrid Monte Carlo: A first-principles approach, Phys. Rev. B **102**, 041124(R) (2020).

[88] R. Iftimie, D. Salahub, D. Q. Wei, and J. Schofield, Using a classical potential as an efficient importance function for sampling from an *ab initio* potential, J. Chem. Phys. **113**, 4852 (2000).

[89] L. D. Gelb, Monte Carlo simulations using sampling from an approximate potential, J. Chem. Phys. **118**, 7747 (2003).

[90] A. Nakayama, T. Taketsugu, and M. Shiga, Speed-up of *ab initio* hybrid Monte Carlo and *ab initio* path integral hybrid Monte Carlo simulations by using an auxiliary potential energy surface, Chem. Lett. **38**, 976 (2009).

[91] K. Kobayashi, Y. Nagai, M. Itakura, and M. Shiga, Self-learning hybrid Monte Carlo method for isothermal–isobaric ensemble: Application to liquid silica, J. Chem. Phys. **155**, 034106 (2021).

[92] R. H. Byrd, P. H. Lu, J. Nocedal, and C. Y. Zhu, A limited memory algorithm for bound constrained optimization, SIAM J. Sci. Comput. **16**, 1190 (1995).

[93] D. Chandler and P. G. Wolynes, Exploiting the isomorphism between quantum theory and classical statistical mechanics of polyatomic fluids, J. Chem. Phys. **74**, 4078 (1981).

[94] D. M. Ceperley, Path-integrals in the theory of condensed helium, Rev. Mod. Phys. **67**, 279 (1995).

[95] B. J. Braams and D. E. Manolopoulos, On the short-time limit of ring polymer molecular dynamics, J. Chem. Phys. **125**, 124105 (2006).

[96] K. Fukui, The path of chemical reactions - the IRC approach, Acc. Chem. Res. **14**, 363 (1981).

[97] G. A. Voth, D. Chandler, and W. H. Miller, Rigorous formulation of quantum transition state theory and its dynamical corrections, J. Chem. Phys. **91**, 7749 (1989).

[98] G. Mills, H. Jónsson, and G. K. Schenter, Reversible work transition state theory: Application to dissociative adsorption of hydrogen, Surf. Sci. **324**, 305 (1995).

[99] J. D. Wrigley, M. E. Twigg, and G. Ehrlich, Lattice walks by long jumps, J. Chem. Phys. **93**, 2885 (1990).

[100] H. Kimizuka, S. Ogata, and M. Shiga, Unraveling anomalous isotope effect on hydrogen diffusivities in fcc metals from first principles including nuclear quantum effects, Phys. Rev. B **100**, 024104 (2019).

[101] H. Kimizuka and M. Shiga, Two distinct non-Arrhenius behaviors of hydrogen diffusivities in fcc aluminum, silver, and copper determined by *ab initio* path integral simulations, Phys. Rev. Mater. **5**, 065406 (2021).

[102] M. Shiga, M. Tachikawa, and S. Miura, *Ab initio* molecular orbital calculation considering the quantum mechanical effect of nuclei by path integral molecular dynamics, Chem. Phys. Lett. **332**, 396 (2000).

[103] M. Shiga, M. Tachikawa, and S. Miura, A unified scheme for molecular orbital theory and path integral molecular dynamics, J. Chem. Phys. **115**, 9149 (2001).

[104] J. T. Bullerjahn, S. von Bulow, and G. Hummer, Optimal estimates of self-diffusion coefficients from molecular dynamics simulations, J. Chem. Phys. **153**, 024116 (2020).

[105] G. J. Martyna, M. L. Klein, and M. Tuckerman, Nosé-Hoover chains: The canonical ensemble via continuous dynamics, J. Chem. Phys. **97**, 2635 (1992).

[106] G. Henkelman, B. P. Uberuaga, and H. Jónsson, A climbing image nudged elastic band method for finding saddle points and minimum energy paths, J. Chem. Phys. **113**, 9901 (2000).

[107] See Supplemental Material at http://link.aps.org/supplemental/10.1103/PhysRevResearch.6.043224 for the NNP prediction data and MD trajectory.

[108] M. Shiga, B. Thomsen, and H. Kimizuka, Inelastic neutron scattering of hydrogen in palladium studied by semiclassical dynamics, Phys. Rev. B **109**, 054303 (2024).

[109] S. Hong and T. S. Rahman, Adsorption and diffusion of hydrogen on Pd(211) and Pd(111): Results from first-principles electronic structure calculations, Phys. Rev. B **75**, 155405 (2007).

[110] J. C. Light and D. Hui Zhang, The quantum transition state wavepacket method, Faraday Discuss. **110**, 105 (1998).